

# Experimental and Theoretical Study of the CD Spectra and Conformational Properties of Axially Chiral 2,2′-, 3,3′-, and 4,4′-Biphenol Ethers

Tadashi Mori,<sup>\*,†,‡</sup> Yoshihisa Inoue,<sup>†</sup> and Stefan Grimme<sup>‡</sup>

Department of Applied Chemistry, Graduate School of Engineering, Osaka University, 2-1 Yamada-oka, Suita 565-0871, Japan, and Theoretische Organische Chemie, Organisch-Chemisches Institut der Universität Münster, Corrensstraße 40, D-48149 Münster, Germany

Received: March 2, 2007

New chiral biphenol ethers (**Biph22**, **Biph33**, and **Biph44**), carrying (*R*)-methylpropyloxy groups at 2,2′-, 3,3′-, and 4,4′-positions of biphenyl, were prepared. The introduced peripheral chiral groups in these biphenol ethers induce an (averaged) axial chirality to give predominant *aR*- or *aS*-rotamers. The chiroptical properties of these axially chiral biphenol ethers in polar and nonpolar solvents were determined experimentally and were compared with the corresponding theoretical values to determine their conformational behavior in solution. Geometry optimization at the DFT-D/TZV2P level and subsequent time-dependent density functional theory (TD-DFT) at the BH-LYP/TZV2P level treatments to obtain rotatory strengths revealed that 6 out of 18 conformers (*aR*-*Tg*-, *aR*-*Tg*+, *aR*-*G*+*t*, *aS*-*Tg*-, *aS*-*Tg*+, and *aS*-*G*+*t*) are crucial to reproduce the experimental circular dichroism (CD) spectra and optical rotations. Although biphenyl molecules are in conformational equilibrium with varying interplanar angles in solution, our static approach to the prediction of the experimental CD spectra is simply based on pairs of thermally populated, local-minimum structures, that is, the dynamic behavior of the systems or the vibrational wave functions are not considered. The relative energies computed at the SCS-MP2/TZVPP level in the gas phase or in acetonitrile solution using the conductor-like screening model (COSMO) were found to be accurate enough to calculate the thermal population of the relevant conformers. Although most of the CD signals mutually cancel out each other between a pair of *aR*- and *aS*-rotamers, the remaining Cotton effects due to a small preference for a single rotamer produce characteristic CD spectra. In general (and somewhat unexpectedly), the delicate cancellation effects in the CD spectra are accurately described by the theoretical approach, and the simulated CD spectra are in excellent agreement with the experimental ones though observed rotatory strengths being always smaller (by 5–20 times) than the theoretical data. Accordingly, slight preferences for the *P* (or *aR*)-configuration for **Biph22** and *M*-configuration for **Biph33** and **Biph44** are determined. The preference for the opposite isomer in the case of **Biph22** is due to larger attractive intramolecular interactions between the chiral alkyl groups. This is also consistent with the lower oxidation potential found for **Biph22** ( $\Delta E \sim 0.1$  V), as compared with those for **Biph33** and **Biph44**. The CT complex formation of **Biph22–44** with various acceptors was also studied by UV–vis and CD spectroscopic methods.

## 1. Introduction

Axial chirality of biaryls was first reported by Kenner and Stubbings in 1921.<sup>1</sup> Since then, the importance of this type of chiral phenomenon, so-called atropisomerism, has attracted much attention for several reasons. For instance, this unique chiral feature is often found in natural products such as vancomycin and knipholone. Axially chiral biaryl compounds, including the well-known BINAP, MOP, and BINOL, are also extremely useful and extensively employed in a variety of asymmetric syntheses as chiral auxiliaries and modifiers of reagents and catalyst.<sup>2</sup> The inter-ring twist angle (and conformation) as well as the rotational barriers associated with the atropisomerism have been intensively studied with the relevant biaryls, terphenyls, and paraphenylenes.<sup>3</sup> Nevertheless, it is still not easy to obtain conformational information reliable enough to predict how and to what extent a twist is induced to a biphenyl

in solution by attaching of a peripheral chiral group and how this affects the chiroptical properties of the molecules.

Electronic circular dichroism (CD)<sup>4</sup> is one of the fundamental properties of chiral molecules. CD spectra are widely used to determine the optical isomerism and secondary/tertiary structure of biomolecules. For simple organic molecules, several empirical rules have been proposed to correlate the observed sign and magnitude of Cotton effects with the absolute configuration of chiral compound.<sup>5</sup> The biphenyl moiety has also been used as a sensible chromophore for determining the absolute configuration of 1,2- and 1,3-diols through the CD spectral examination.<sup>6</sup> Despite that, the relationship between the molecular structure and the observed Cotton effects in the CD spectrum is not fully understood and the frequently used empirical rules are occasionally not very reliable particularly in less conventional cases.<sup>7</sup> Thus, more accurate theoretical treatments of chiroptical properties are indispensable for elucidating and simulating the observed circular dichroism of chiral molecules. In this relation, the time-dependent density functional theory (TD-DFT) calculations of chiroptical properties, such as optical

\* To whom correspondence should be addressed. Fax: +81-6-6879-7923. E-mail: tmori@chem.eng.osaka-u.ac.jp.

<sup>†</sup> Osaka University.

<sup>‡</sup> Universität Münster.

rotatory dispersions,<sup>8</sup> vibrational circular dichroism,<sup>9</sup> and electronic CD spectra,<sup>10,11</sup> have recently been applied successfully to the absolute configuration assignment of small- to medium-sized chiral organic molecules.

We have recently reported an application of the TD-DFT calculations to the CD spectra of a large chiral molecule, which successfully interpret its conformational variation in solution.<sup>12</sup> Herein, we will apply these state-of-the-art methods to the differently substituted conformationally flexible biphenol ethers (**Biph22–44**) to examine how peripheral chiral groups affect the axial chirality of the molecules. By comparing the theoretical CD spectra calculated by the BH-LYP/TZV2P method with the experimental ones, it has turned out that most of the CD signals arising from the rotamers are mutually cancelled out to leave the oppositely signed signals of *P*-chirality for **Biph22** and of *M*-chirality for **Biph33** and **Biph44**. The effects of oxidation on the axial chirality are also examined experimentally and theoretically.

## 2. Experimental Methods and Theoretical Calculations

**Preparation of Biph22, Biph33, and Biph44 by Mitsunobu Reaction.**<sup>13</sup> *Typical Procedure.* Biphenol (3.72 g, 20 mmol), triphenylphosphine (11.0 g, 42 mmol, 2.1 equiv), and (*S*)-(+)-2-butanol (2.96 g, 40 mmol, 2.0 equiv) were dissolved in THF (400 mL), to which a THF solution of diisopropyl azodicarboxylate (8.5 mL, 44 mmol, 2.2 equiv in 100 mL THF) was added dropwise over 2 h, and the mixture was stirred for 20 h at ambient temperature under argon atmosphere. The resulting solution was concentrated and the residue was purified by column chromatography over silica gel with a hexane-diethyl ether (50:1) eluent to give the desired products.

(–)-(***R,R***)-**Biph22**. Yield: 2.09 g, 35%. Colorless oil.  $\delta_{\text{H}}$ : 0.77 (6H, t,  $J = 7.4$  Hz), 1.13 (6H, d,  $J = 6.2$  Hz), 1.43 (2H, pseudo sept,  $J = 7.6$  Hz), 1.54 (2H, pseudo sept,  $J = 7.6$  Hz), 4.12 (2H, sxt,  $J = 6.2$  Hz), 6.93 (2H, d,  $J = 7.6$  Hz), 6.93–6.96 (2H, m), and 7.21–7.27 (4H, m). Peaks of the minor conformer were also observed at 0.78 (9H, t,  $J = 7.6$  Hz) and 1.14 (9H, d,  $J = 6.4$  Hz), in an approximately 4:1 ratio.  $\delta_{\text{C}}$ : 9.64, 19.15, 29.29, 75.85, 115.10, 120.14, 128.06, 130.01, 132.18, and 155.75. Peaks of the minor conformer were also observed at 29.27, 9.66, and 75.88. MS (EI, direct):  $m/z = 298$  ( $M^+$ , 14%), 187 (14), and 186 (100). HRMS (EI): 298.1928.  $\text{C}_{20}\text{H}_{26}\text{O}_2$  requires 298.1933. EA: Found: C, 80.34; H, 8.78%. Calcd for  $\text{C}_{20}\text{H}_{26}\text{O}_2$ : C, 80.50; H, 8.78; O, 10.72. Specific rotation:  $[\alpha]_{\text{D}}^{25} -55.3 \pm 5.6^\circ$  ( $c$  0.10,  $\text{CHCl}_3$ ).

(–)-(***R,R***)-**Biph33**. Yield: 4.80 g, 80%. Colorless oil.  $\delta_{\text{H}}$ : 0.98 (6H, t,  $J = 7.4$  Hz), 1.30 (6H, d,  $J = 6.4$  Hz), 1.63 (2H, pseudo sept,  $J = 7.6$  Hz), 1.76 (2H, pseudo sept,  $J = 7.6$  Hz), 4.34 (2H, sxt,  $J = 6.2$  Hz), 6.86 (2H, ddd,  $J = 8.0, 2.0, 1.2$  Hz), 7.11–7.16 (4H, m), and 7.29 (2H, t,  $J = 8.0$  Hz).  $\delta_{\text{C}}$ : 9.92, 19.42, 29.36, 75.16, 114.76, 115.09, 119.54, 129.78, 142.82, and 158.68. HRMS (EI): 298.1931.  $\text{C}_{20}\text{H}_{26}\text{O}_2$  requires 298.1933. EA: Found: C, 80.46; H, 8.86%. Calcd for  $\text{C}_{20}\text{H}_{26}\text{O}_2$ : C, 80.50; H, 8.78; O, 10.72. Specific rotation:  $[\alpha]_{\text{D}}^{25} -18.1 \pm 6.0^\circ$  ( $c$  0.10,  $\text{CHCl}_3$ ).

(–)-(***R,R***)-**Biph44**. Yield: 4.79 g, 80%. Mp: 37–38 °C.  $\delta_{\text{H}}$ : 0.99 (6H, t,  $J = 7.4$  Hz), 1.31 (6H, d,  $J = 6.2$  Hz), 1.63 (2H, pseudo sept,  $J = 7.8$  Hz), 1.77 (2H, pseudo sept,  $J = 7.8$  Hz), 4.31 (2H, sxt,  $J = 6.2$  Hz), 6.93 (4H, AA'XX',  $J = 8.8, 2.4$  Hz), and 7.44 (4H, AA'XX',  $J = 8.8, 2.4$  Hz).  $\delta_{\text{C}}$ : 9.97, 19.46, 29.37, 75.29, 116.25, 127.84, 133.46, and 157.46. MS (EI, direct):  $m/z = 298$  ( $M^+$ , 20%), 187 (13), and 186 (100). HRMS (EI): 298.1930.  $\text{C}_{20}\text{H}_{26}\text{O}_2$  requires 298.1933. EA: Found: C, 80.44; H, 8.71%.  $\text{C}_{20}\text{H}_{26}\text{O}_2$ : C, 80.50; H, 8.78; O, 10.72. Specific rotation:  $[\alpha]_{\text{D}}^{25} -31.3 \pm 4.7^\circ$  ( $c$  0.10,  $\text{CHCl}_3$ ).

**Technical Details of the Computations.** All calculations were performed on Linux-PCs using the TURBOMOLE 5.8 program suite.<sup>14</sup> The resolution of identity (RI) approximation<sup>15,16</sup> was employed in all DFT-D-B-LYP calculations, and the corresponding auxiliary basis sets were taken from the TURBOMOLE basis set library. The program module escf<sup>17</sup> has been used in the TD-DFT treatments. All conformers were fully optimized at the dispersion-corrected DFT-D-B-LYP level<sup>18</sup> without any symmetry constraint, using an atomic orbital (AO) basis set of valence triple- $\zeta$  quality with two sets of polarization functions (2d2p, denoted as TZV2P; in standard notation: H, [3s2p], C/O, [5s3p2d]) and numerical quadrature grid m4. All conformations of the chiral alkyl group were checked for **Biph22**, and it was found that three major conformations (*Tg*-, *Tg*+, and *G+t*) in each rotamer are important. Thus, only these conformations were considered for **Biph33** and **Biph44** for simplicity. Subsequent single-point energy calculations were performed with the spin-component-scaled (SCS)-MP2 method<sup>19,20</sup> with a TZVPP basis set that has additional f and d functions on non-hydrogen and hydrogen atoms, respectively. It has been shown that a simple modification of the standard MP2 scheme, termed SCS-MP2, leads to dramatic improvements in accuracy, particularly for molecules with weak interactions where standard DFT method fails.<sup>21</sup> The method is expected to provide the most accurate relative energies (comparable to the computationally very demanding CCSD(T) calculations) and was thus used to obtain the final Boltzmann distribution (always at 298 K) of the conformers. All excited-state calculations have been performed at the optimized ground-state geometries. The results thus correspond to vertical transitions, and the excitation energies can be approximately identified as the band maxima in the experimental spectra. The CD (and UV-vis) spectra were simulated on the basis of time-dependent density functional theory (TD-DFT) with the BH-LYP<sup>22</sup> functional and employing the TZV2P basis set. Because this basis is already quite large, we were unable to further check basis set incompleteness effects. However, the differences between length and velocity-gauge representations are found to be very small (mostly less than  $1 \times 10^{-40}$  cgs unit) which indicates sufficient basis set saturation. The CD spectra were simulated by overlapping Gaussian functions for each transition where the width of the band at  $1/e$  height is fixed at 0.4 eV and the resulting intensities of the combined spectra were scaled to the experimental values. As usual, the calculated band intensities are larger than their experimental counterparts. The somewhat smaller scaling factor used ( $1/5-1/20$  instead of normally  $1/2-1/3$ ) is probably due to a more complete cancellation of the CD bands between the various conformers under the experimental conditions and our ignorance of the dynamic behavior of the systems (or, in other words, the neglect of averaging the chiroptical properties over vibrational wavefunctions) in the present approach. Because of a systematic overestimation of the transition energies compared to the experiment in the BH-LYP calculations, the spectra were uniformly shifted by 0.5 eV. See ref 11 for more theoretical details on the simulation of CD spectra. The optical rotations at the sodium-D line wavelength were also calculated at the TDDFT/BH-LYP method using Dunning's<sup>23</sup> aug-cc-pVDZ basis sets for the same optimized structures. Rotational strengths are calculated using both length and velocity representations, but the numerically more robust values from length-gauge representation were used throughout the text. It is known that in the absence of gauge-invariant atomic orbitals (GIAOs), these are origin-dependent and origin-independent, respectively. Strictly speaking, the calculated

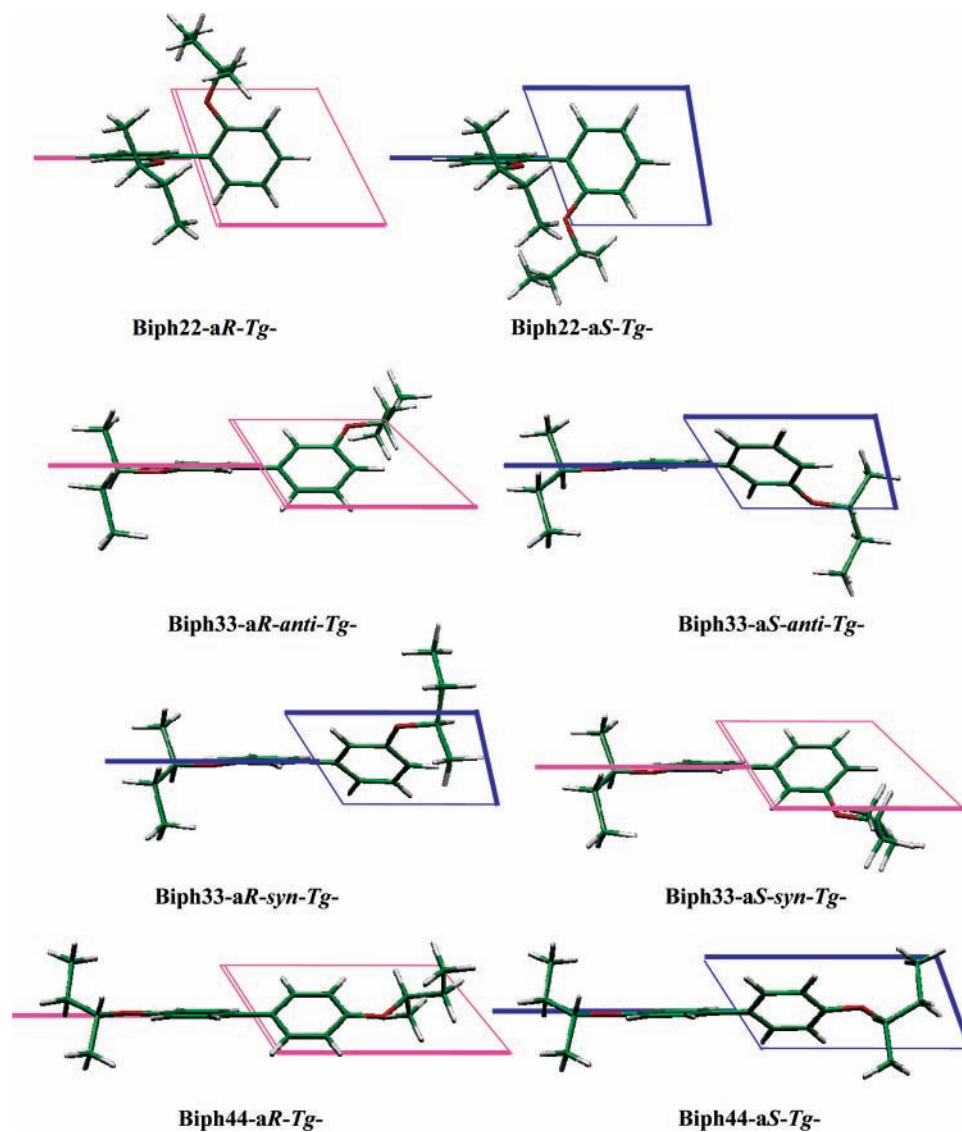
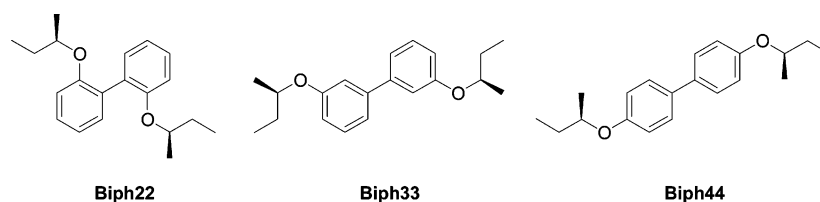


**Figure 1.** Front view of the DFT-D-B-LYP/TZVP-optimized, most abundant *Tg*- conformers of **Biph22**, **Biph33** (anti and syn), and **Biph44**. Magenta and navy planes stand for the positive and negative twists, respectively.

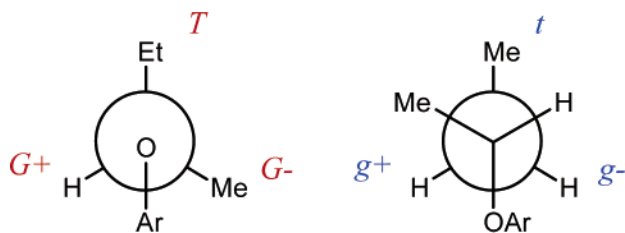
#### CHART 1: Chiral Biphenol Ethers



optical rotations and circular dichroisms can only be compared to experimental values when they are origin-independent, but the length and velocity rotational strengths converge to the same value in the complete basis set limit. With our relatively large triple- $\zeta$  type AO basis sets, the differences between both representations were negligible. The effect of the solvent on the distribution of the conformers was also addressed by application of the conductor-like screening model (COSMO).<sup>24</sup> All single-point energy calculations were performed with COSMO as implemented in the TURBOMOLE program suite. The dielectric constant ( $\epsilon$ ) of 36.64 in acetonitrile and optimized atomic radii for the construction of the molecular cavity (C, 2.00; O, 1.72; H, 1.30 Å) were used.

#### 3. Results and Discussion

**Preparation of Chiral Biphenol Ethers.** A series of symmetrically substituted biphenol ethers **Biph22**, **Biph33**, and **Biph44** (Chart 1) were synthesized by the Mitsunobu reaction of the corresponding biphenols with (*S*)-2-butanol in tetrahydrofuran. The smallest chiral group was selected to examine the ability of inducing axial chirality to a biphenyl chromophore and also to test the capability of the present conformational analysis that combines the experimental and calculated CD spectra, through which we can verify whether or not the small but significant differences in energy/population between *aR*- and *aS*-isomers can be appropriately deduced. The yields of the chiral ethers were fair to good, while the monosubstituted ether

**CHART 2: Conformations at *O*–*C* (chiral) and *C* (chiral)–*C* (ethyl) Bonds<sup>a</sup>**

<sup>a</sup> Left: trans and two gauche isomers defined by the orientation of ethyl substituent in the chiral group (*T*, *G*<sup>+</sup>, and *G*<sup>-</sup>). Right: trans and two gauche isomers defined by the orientation of methyl substituent in the ethyl group (*t*, *g*<sup>+</sup>, and *g*<sup>-</sup>).

was obtained as the major product when 2,2'-biphenol was used as the substrate, for which the steric hindrance of the 2,2'-disubstituted product should be responsible. Because of this crowdedness, a pair of diastereomers (rotamer) were observed for **Biph22** on the NMR time scale. Heating the solution up to 100 °C caused some peak broadening but did not lead to coalescence of these signals (see Figure S2 in the Supporting Information for details). This indicates that the interconversion between the conformers is slow even at this temperature. It has been reported that a pair of such diastereomers can be separated in some cases and also that an independent preparation of diastereomeric 2,2'-bis(phenyloxadiazolyl)biphenyl is possible.<sup>25</sup> However, we were unable to separate the diastereomers of **Biph22** despite considerable effort, and hence we decided to use the diastereomeric mixture for the CD experiments throughout the study.

**Geometrical Optimization and Calculation of the Circular Dichroism Spectra of Chiral Biphenol Ethers by the TD-DFT Method. A Test for the Conformational Variance of Biph22.** We have recently developed an empirical dispersion correction scheme for efficient DFT calculations by adding pairwise  $-C_6/R^6$  potentials to describe van der Waals (vdW) interactions (DFT-D).<sup>18</sup> This dispersion-corrected DFT method is a very efficient practical alternative to computationally very demanding electron correlation methods and has successfully been applied to noncovalently bound intermolecular complexes<sup>26</sup> as well as large host-guest molecules.<sup>27,28</sup> All of the geometrical optimizations of chiral biphenol ethers (**Biph22–44**) were performed at the DFT-D-B-LYP/TZV2P level, which were followed by the single-point energy calculation at the SCS-MP2/TZVPP level.<sup>20,21</sup> The relative populations of the conformers reported in this work are based on the Boltzmann distributions calculated from these SCS-MP2 energies (DFT-D and uncorrected standard DFT energies were used only for comparison purposes).

To check the effect of the conformation of the terminal alkyl group on the relative energy as well as on the UV-vis/CD spectra, we first comprehensively studied all of the possible conformations of **Biph22**. The choice of **Biph22**, rather than **Biph33** or **Biph44**, for this assessment is because the relative energies are more severely affected by intramolecular interaction between the adjacent ortho substituents of **Biph22**. In addition to the rotational conformations associated with the aryl-aryl bond (denoted as *aR*- and *aS*-isomers,<sup>29</sup> Figure 1 for *Tg*-conformation), there are nine possible conformations for each rotamer because of the orientational isomerism in the terminal alkyl group. Chart 2 illustrates the possible conformations associated with the *O*–*C* (chiral) and *C* (chiral)–*C* (ethyl) bonds, which are hereafter denoted as *T* (trans), *G*<sup>+</sup> (gauche 1), and *G*<sup>-</sup> (gauche 2) in the former case and *t*, *g*<sup>+</sup>, *g*<sup>-</sup>

(lowercase) in the latter case. Combination of different conformations in the two aromatic rings was ignored for simplicity. This assumption turned out to be acceptable as the experimental CD spectra are nicely reproduced by the calculation incorporating these conformers (vide infra).

It turned out that only three major conformers for each rotamer are practically relevant for the calculation of the CD spectrum. In addition to the most stable *aR-G+t* isomer, all the conformations that possess  $\Delta E < 2$  kcal/mol above the lowest are taken into account. The other 12 minor conformations consist of ~15% in total, but the relative population of each conformation never amounts to 5%. In addition, the possible Cotton effects of the minor conformers are expected to mostly cancel out (vide infra) since the populations to the corresponding *aR*- and the *aS*-isomers are almost equal. For a full table of the relative energies as well as the populations of all the conformations of **Biph22**, see Table S1 in Supporting Information.

The present-day TD-DFT implementation regarding optical activities such as CD spectra<sup>10,11,30</sup> has been successfully applied recently to the assignment of absolute configuration and conformation of chiral organic molecules. Consequently, we performed the TD-DFT calculations for all of the 18 conformers at the BH-LYP/TZV2P level to simulate the UV-vis and CD spectra of **Biph22** in each conformation. The choice of the functional and the basis sets is based on previous experience.<sup>12,31</sup> While the UV-vis spectra predicted for all of these conformers were essentially the same (data not shown), the calculated CD spectra were significantly different from each other (Figure S8 in Supporting Information). Most importantly, the Cotton effects of *aR*- and *aS*-rotamers are opposite in sign and the CD spectra of the rotamers are almost mirror-imaged (e.g., *aR-Tg-* versus *aS-Tg-*). Thus, the contribution from the minor component is mostly cancelled out, and therefore the CD spectra predicted by considering only the major conformations are incredibly similar to the ones that incorporate all the conformers, except for the slight decrease in peak height (Figure S9 in Supporting Information). Accordingly, only the six conformations (*aR-Tg-*, *aR-Tg+*, *aR-G+t*, *aS-Tg-*, *aS-Tg+*, and *aS-G+t*) with respect to the chiral group are hereafter considered in the CD calculation of **Biph22–44**.

**Experimental and Theoretical UV-Vis and CD Spectra of Chiral Biphenol Ethers.** The UV-vis and CD spectra of **Biph22–44** were obtained with a conventional UV-vis/CD apparatus using a 1.0 cm square cuvette for 0.05 mM solutions in methylenecyclohexane and acetonitrile at 25 °C. These data are compared with the theoretical UV-vis and CD spectra.

(a) **Biph22.** Table 1 summarizes the results of the geometrical optimization of the three major conformers (*Tg+*, *Tg-*, and *G+t*) of each **Biph22** rotamer. The geometry optimization was performed at the DFT-D-B-LYP/TZV2P level, followed by single-point energy calculation at the SCS-MP2/TZVPP level. The representative optimized conformations (*aR-Tg-* and *aS-Tg-*) are illustrated in Figure 1 (top). The interplanar dihedral angles between the two phenol ether moieties are relatively large and mostly in the range of 65–70°. These values are in good agreement with the <sup>13</sup>C NMR-estimated twist angle of 73° for 2,2'-dimethylbiphenyl.<sup>32</sup> An exception is the *aS-Tg-* isomer which shows a remarkably large twist angle of 91°, probably because of a larger steric repulsion between the chiral alkyl groups.

The calculation of the UV-vis and CD spectra for each conformer of **Biph22** was performed by using the TD-DFT method with the BH-LYP functional and the same triple- $\zeta$  basis sets (TZV2P). The individual theoretical spectra are shown in

**TABLE 1: Summary of the Calculated Structures, Relative Energies, and Thermal Boltzmann Populations for the Three Biphenol Ethers<sup>a</sup>**

	gas phase					in acetonitrile (COSMO)													
	twist angle/ <sup>o</sup>	calculated optical rotation/ <sup>o</sup> <sup>c</sup>	SCS-MP2 energy/Hartree <sup>b</sup>	$\Delta E_{\text{SCS-MP2}}$ /kcal mol <sup>-1</sup>	% population	$\Delta E_{\text{DFT-D}}$ /kcal mol <sup>-1</sup>	% population	$\Delta E_{\text{DFT}}$ /kcal mol <sup>-1</sup>	% population	$\Delta E_{\text{SCS-MP2}}$ /kcal mol <sup>-1</sup>	% population	$\Delta E_{\text{DFT-D}}$ /kcal mol <sup>-1</sup>	% population						
<b>Biph22</b>																			
<i>aR-Tg+</i>	67.1	-1021	-926.2568	1.62	9.5	0.78	16.5	3.89	1.1	1.36	9.8	0.53	16.1						
<i>aR-Tg-</i>	67.5	-2032	-926.2594	≡ 0	47.7	≡ 0	35.8	≡ 0	54.4	≡ 0	38.2	≡ 0	27.4						
<i>aR-G+t</i>	69.5	-1327	-926.2557	2.32	4.7	1.63	7.0	1.24	15.8	1.23	11.1	0.69	13.7						
<i>aS-Tg+</i>	-69.5	1174	-926.2563	1.95	6.8	1.61	7.2	2.49	4.5	1.79	6.4	1.44	6.5						
<i>aS-Tg-</i>	-90.8	-203	-926.2581	0.76	22.2	0.51	21.5	1.40	13.5	0.86	16.2	0.55	15.7						
<i>aS-G+t</i>	-65.1	1023	-926.2567	1.65	9.1	1.09	12.0	1.62	10.7	0.73	18.4	0.28	20.7						
<i>R/S (P/M<sup>d</sup>) ratio</i>					61.9:38.1				59.2:40.7				71.3:28.7			59.1:40.9			57.1:42.9
<b>Biph33</b>																			
<i>aR-anti-Tg+</i>	140.9	-62	-926.2561	2.25	2.0	1.86	2.6	2.43	1.7	2.41	1.5	2.02	1.9						
<i>aR-anti-Tg-</i>	141.1	-336	-926.2597	0.02	18.3	0.05	15.5	0.02	18.5	0.09	15.2	0.13	12.7						
<i>aR-anti-G+t</i>	141.6	67	-926.2575	1.38	4.7	0.90	6.6	1.41	4.6	0.78	7.6	0.40	9.7						
<i>aR-syn-Tg+</i>	-38.6	-205	-926.2561	2.26	2.0	1.84	2.6	2.40	1.7	2.37	1.6	1.97	2.0						
<i>aR-syn-Tg-</i>	-38.5	-496	-926.2597	≡ 0	18.7	≡ 0	16.2	≡ 0	19.0	0.05	15.9	0.07	13.5						
<i>aR-syn-G+t</i>	-38.6	-136	-926.2575	1.38	4.7	0.93	6.5	1.44	4.5	0.76	7.8	0.40	9.7						
<i>aS-anti-Tg+</i>	-141.4	-26	-926.2561	2.29	1.9	1.85	2.6	2.39	1.8	2.42	1.5	1.98	2.0						
<i>aS-anti-Tg-</i>	-141.5	-277	-926.2597	0.02	18.3	0.00	16.3	0.00	19.0	≡ 0	16.7	≡ 0	14.5						
<i>aS-anti-G+t</i>	-141.5	54	-926.2575	1.39	4.7	0.93	6.4	1.44	4.5	0.78	7.7	0.41	9.6						
<i>aS-syn-Tg+</i>	38.9	229	-926.2561	2.28	1.9	1.86	2.5	2.43	1.7	2.42	1.5	2.01	1.9						
<i>aS-syn-Tg-</i>	38.8	-172	-926.2597	0.02	18.3	0.04	15.7	0.02	18.5	0.07	15.5	0.11	13.0						
<i>aS-syn-G+t</i>	38.6	156	-926.2575	1.38	4.7	0.91	6.6	1.43	4.5	0.78	7.7	0.40	9.7						
<i>R/S ratio</i>					50.3:49.7				49.9:50.1				50.0:50.0			49.6:50.4			49.4:50.6
<i>P/M ratio<sup>d</sup></i>					49.9:50.1				49.4:50.6				49.6:50.4			49.0:51.0			48.9:51.1
<b>Biph44</b>																			
<i>aR-Tg+</i>	37.2	-4234	-926.2558	2.24	3.9	1.86	5.1	2.35	3.5	2.31	3.1	1.90	4.0						
<i>aR-Tg-</i>	37.2	-1188	-926.2593	0.01	36.2	0.05	30.8	≡ 0	37.2	≡ 0	31.7	≡ 0	26.4						
<i>aR-G+t</i>	36.8	134	-926.2572	1.32	9.7	0.88	13.5	1.35	9.6	0.70	15.8	0.27	20.1						
<i>aS-Tg+</i>	-36.9	-306	-926.2558	2.24	3.9	1.85	5.1	2.34	3.6	2.33	3.1	1.90	4.0						
<i>aS-Tg-</i>	-36.8	-947	-926.2593	≡ 0	36.5	≡ 0	32.5	0.00	37.2	0.06	29.9	0.02	25.9						
<i>aS-G+t</i>	-36.8	404	-926.2572	1.32	9.8	0.92	13.0	1.43	8.9	0.66	16.3	0.29	19.8						
<i>R/S (P/M<sup>d</sup>) ratio</i>					49.8:50.2				49.3:50.7				50.3:49.7			50.7:49.3			50.4:49.6

<sup>a</sup> Boltzmann populations (298 K) based on the relative energies in the gas phase and in acetonitrile with COSMO calculations. <sup>b</sup> SCS-MP2/TZVPP single-point energies for DFT-D-B-LYP/TZV2P optimized structures. <sup>c</sup> Calculated optical rotations at the BH-LYP/aug-cc-pVDZ level. <sup>d</sup> Relative contribution of the conformations with positive twist angle versus those with negative twist angle.

Figure 2 (top left), which clearly indicate that the spectra for *aR*- and *aS*-rotamers are mostly mirror-imaged. The *aS-Tg*-isomer, which is sterically more crowded and thus bears an increased twist angle, shows a slightly sluggish CD profile compared to the others. However, the overall patterns of the CD spectra, that is, the negative–positive–negative Cotton effect sequence for *aR*-rotamers and the oppositely signed sequence for the antipodal *aS*-rotamers, uniformly hold. The delicate balance between the *aR* and *aS* rotamer populations, and thus the calculation of accurate relative energies, is a very important issue to properly reproduce the experimental CD spectra.

Accordingly, accurate SCS-MP2 energies were used to estimate the relative population of the isomers, and the results are shown in Table 1. The populations predicted by the SCS-MP2 and the DFT-D methods are very similar. At least the stability order of the conformers completely agrees for both methods, although a higher preference for the more stable isomers is noted for SCS-MP2. In contrast, standard DFT failed to predict the correct ordering of the relative energies (and population) because of the known defect of common density functionals to describe dispersion (van der Waals) interactions; these problems have been recently pointed out by many authors.<sup>21,33</sup> This finding also supports the reliability of the DFT-D method for the geometrical optimization of the present system.

The most abundant isomer bears the *aR-Tg-* conformation, while the corresponding rotamer (*aS-Tg-*) is less stable by about

0.5 kcal/mol because of the larger sterical repulsion in the *aS*-isomer. The overall *aR/aS* ratio determined is  $\sim 6:4$ , which is roughly equal to the ratio obtained by the <sup>1</sup>H NMR analysis (ca. 8:2).

Figure 3 shows a comparison of the experimental and the simulated UV–vis (left) and CD spectra (right) for **Biph22** obtained by averaging the contributions of six conformers. The three major bands are correctly predicted in the theoretical UV–vis spectrum, while the transition energies and the oscillator strengths deviated slightly. More importantly, the present methods show excellent performance in predicting the theoretical CD spectrum, which almost perfectly agrees in shape with the experimental spectrum. The calculated band intensities are usually larger than the experimental ones, and thus the theoretical spectrum was scaled to <sup>1</sup>/<sub>10</sub> to fit the experimental values. The experimental UV–vis spectra of **Biph22–Biph44** can be reproduced by the same theory with much smaller scaling factor ( $1 \sim 1/2$ ). The somewhat smaller scaling factor used is probably due to a more complete cancellation of the CD bands between the various conformers and also to the neglect of the dynamic behavior of the substrate conformations in our static approach. However, the apparent three Cotton effect peaks of a negative–positive–negative sequence were perfectly reproduced in sign and in relative band intensity, indicating the appropriateness of our combined approach, that is, the SCS-MP2 calculation of the relative energy, the TD-DFT calculation of the CD spectra, as well as the DFT-D optimization of the chiral biphenol ether **Biph22**. Thus, it is clear that the *aR*- (or *P*-), rather than *aS*-

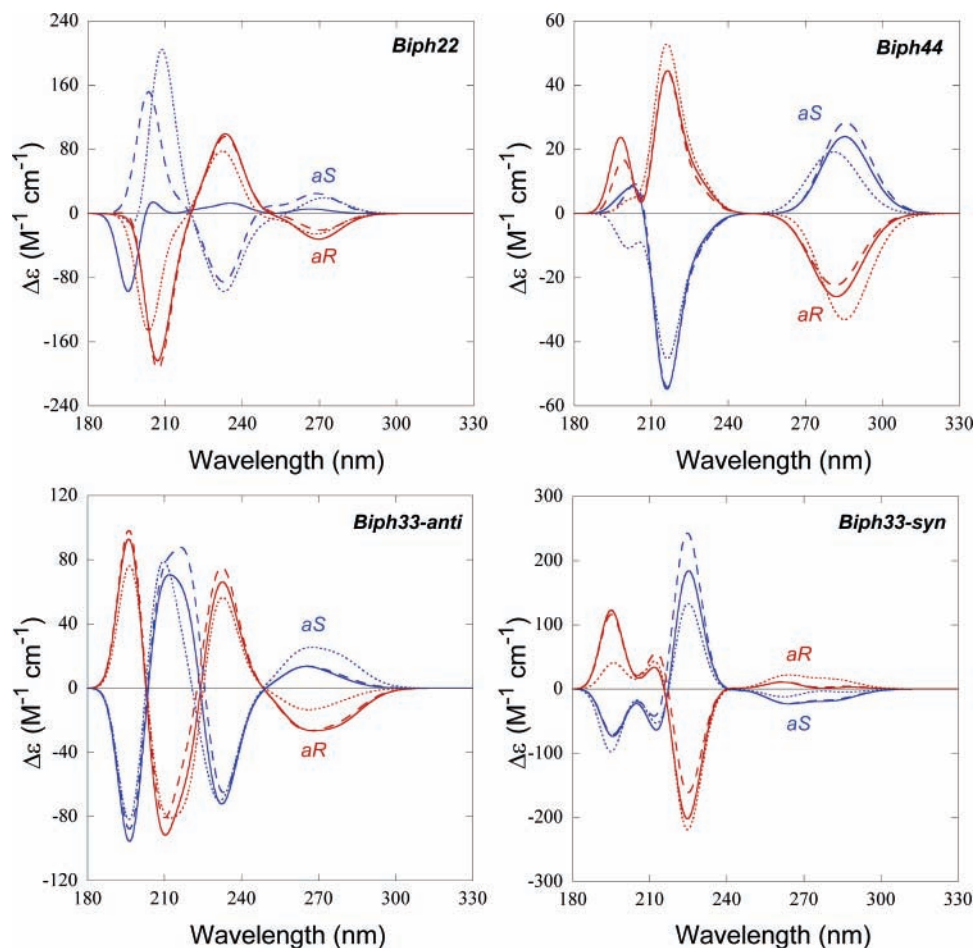


**Figure 2.** Calculated CD spectra of **Biph22** (top, left), **Biph33** (bottom), and **Biph44** (top, right) for selected conformers. Red, solid: *aR-Tg-*; red, dotted: *aR-Tg+*; red, hashed: *aR-G+t*; blue, solid: *aS-Tg-*; blue, dotted: *aS-Tg+*; blue, hashed: *aS-G+t*. For **Biph33**, anti (left) and syn (right) conformers are shown separately for clarity.

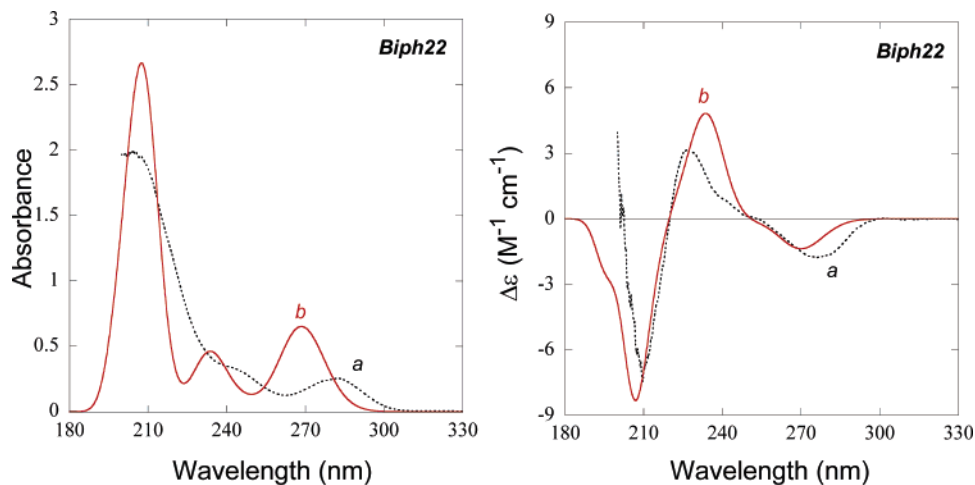


**Figure 3.** Comparison of calculated and experimental UV-vis/CD spectra of **Biph22**. Left: (a) Experimental UV-vis spectrum (0.05 mM in methylcyclohexane at 25 °C). (b) Calculated UV-vis spectrum obtained by averaging the six conformers. Right: (a) Experimental CD spectrum. (b) Calculated CD spectra of **Biph22** obtained by averaging the six conformers with a scaled intensity ( $1/10$ ).

(or *M-*), rotamers are preferred for (*R,R*)-**Biph22** in solution under the experimental conditions. This is in contrast to the slight preference for the *M*-isomers observed for **Biph33** or **Biph44** (vide infra), which is probably due to the larger interactions between the chiral alkyl groups in **Biph22**. Judging from the superlative agreement of the theoretical and the experimental CD spectra, we may conclude that the relative *aR/aS* ratio is very close to  $\sim 60:40$ .

(b) **Biph33**. The geometrical optimization of the selected conformers of the 3,3'-disubstituted derivative **Biph33** was also performed at the DFT-D-B-LYP/TZV2P level. In addition to the conformations based on the trans/gauche orientations of the alkyl groups as was the case in **Biph22**, there are four possible conformations (rotamers) associated with the interplanar twist angle (for a typical example, see the *Tg-* isomer in Figure 1, middle). We use the combination of *aR/aS* and syn/anti

**TABLE 2: Relative *aS/aR* Preference in Each Conformer<sup>a</sup>**

medium		<b>Biph22</b>		<b>Biph33 (anti)</b>		<b>Biph33 (syn)</b>		<b>Biph44</b>	
		$\Delta E_{\text{SCS-MP2}}$ / kcal mol <sup>-1</sup>	<i>aR/aS</i> ratio						
gas phase	<i>Tg+</i>	+0.332	41.8:58.2	+0.041	49.0:51.0	+0.025	49.6:50.6	-0.000	50.0:50.0
	<i>Tg-</i>	+0.765	31.8:68.2	+0.003	49.9:50.1	+0.019	49.5:50.5	-0.008	50.2:49.8
	<i>G+t</i>	-0.663	66.0:34.0	+0.012	49.7:50.3	+0.002	49.9:50.1	-0.005	50.1:49.9
MeCN (COSMO)	<i>Tg+</i>	+0.423	39.6:60.4	+0.012	49.7:50.3	+0.045	48.9:51.1	+0.021	49.5:50.5
	<i>Tg-</i>	+0.858	29.8:70.2	-0.089	52.2:47.8	+0.022	49.4:50.6	+0.058	48.6:51.4
	<i>G+t</i>	-0.500	62.3:37.7	-0.007	50.2:49.8	+0.020	49.5:50.5	-0.031	50.8:49.2

<sup>a</sup> Boltzmann population (298 K) based on the relative SCS-MP2/TZVPP energies in the gas phase and in acetonitrile with COSMO calculations.

nomenclatures for these conformers, where the anti isomers possess larger twist angles between the aromatic planes on the basis of the direction of the attached alkoxy group ( $\theta > 90^\circ$ ). The syn isomers were not found as stable conformations in the case of **Biph22** because of the larger steric hindrance between the alkoxy groups. Thus, compared with achiral analogs, possible conformers of **Biph22–Biph44** are doubled in number. Details of the results of the calculations for 12 out of 36 conformations are summarized in Table 1. The twist angles are in the range of 38–40° in all of the conformations, which are in good agreement with the reported interplanar angles of 44° determined by an electron-diffraction experiment with the parent biphenyl.<sup>34</sup>

Quite interestingly, the *aR-syn-Tg-* isomer was the most stable among the conformations examined, while all of the *aS-syn-Tg-* counterparts and the *Tg-* conformers of the anti forms have comparable stabilities, where  $\Delta E_{\text{SCS-MP2}} \sim 0.02$  kcal/mol. In this case, most of the rotamers are fabulously balanced in energy (*aR/aS*  $\sim$  50:50), and thus only a tiny *aR* preference (50.3:49.7) was found on the basis of the SCS-MP2 energies. This *aR* preference, however, is in contrast to the small *aS* preference predicted by the DFT-D energies (49.9:50.1). It is more important for this substrate that the *P/M* ratio, the relative contribution of the conformations with positive versus negative twist angles, is always slightly smaller than unity independent of the choice of calculation methods (SCS-MP2 vs DFT-D). The relative energies and the population between the conformers can also be correctly predicted for **Biph33** by standard DFT, which is in contrast to the **Biph22** case. Thus, the *P/M* classification is much more reasonable for the prediction of the conformational preference as well as the UV–vis/CD spectra; all the *P* (or the *M*) isomers possess the same structural trends as shown in Figure 1 (positive and negative interplanar twist angles are represented as magenta and navy plates, respectively). The CD spectra are also calculated for all conformations at the TD-DFT-BH-LYP/TZV2P level (Figure 2, bottom). As clearly seen, all the *P* isomers (*aR-anti-* and *aS-syn-*conformers) show the first-negative, second-positive Cotton effects, and vice versa for the *M* isomers. Consequently, the accurate estimation of the relative contribution (energies) is obligatory to predict the CD spectra of **Biph33** correctly.

The prediction of the UV–vis or CD spectra of **Biph33** and **Biph44** is more challenging than that of **Biph22**, since as can be seen from Table 2, the relative *aS/aR* preferences are almost balanced ( $|\Delta E| < 0.1$  kcal/mol) when the conformations of the terminal alkyl groups are fixed. Nevertheless, our approach performs exceptionally well for both **Biph33** and **Biph44** (vide infra). The theoretical (averaged) and experimental UV–vis and CD spectra of **Biph33** are compared in Figure 4. The computed intensities of the calculated UV and CD spectra are scaled to  $1/2$  and  $1/20$  for better comparison. The three main transitions are appropriately predicted by the theory in the UV–vis spectra, with some deviation of the transition energies. The first two

transitions appear as an overlapping broad peak in the calculated UV–vis spectrum, since the first and the second transitions are blue- and red-shifted, respectively, compared to the experimental ones. The calculated CD spectrum obtained by a Boltzmann distribution averaging of the 12 individual spectra reasonably reproduces the experimental CD spectrum in methylcyclohexane. The relatively small scaling factor ( $1/20$ ) necessary for **Biph33** is probably due to the broader variety of conformations involved in comparison to the **Biph22** and **Biph44** cases. Indeed, experimentally the CD intensity of **Biph33** is almost 1 order of magnitude smaller than that of **Biph22**. A slight deviation of the second positive Cotton effect (in the theoretical spectrum) may rationalize the inconsistent relative strength of the first negative Cotton effect at least in part. However, the overall good agreement of the CD patterns in theory and experiment demonstrates the reliability of the present methods. The slight preference for the *M* isomers in solution, as predicted by the SCS-MP2 calculations, was thus confirmed.

(c) **Biph44**. The geometry optimization and UV–vis/CD spectral calculation were similarly performed for **Biph44** (Table 1, Figures 1, 2, and 5). The interplanar twist angles are  $\sim 37^\circ$ , which is in good agreement with the experimental value (44°) of biphenyl.<sup>34</sup> These equilibrium angles are slightly smaller than those for **Biph33**. The overall preference for the *aR-(M)*-isomers over the *aS-(P)*-isomers was very subtle (50.2:49.8), and the *aS/aR* ratios for respective conformers in the alkyl group are very close to unity (Table 2). As was the case for **Biph33**, the observed CD is very weak, that is,  $\Delta\epsilon$  values are generally less than  $\pm 1$  M<sup>-1</sup> cm<sup>-1</sup>. This is not surprising because the chiral groups are located in the position most distal from the twisting C–C bond and thus the chiral induction is not very effective for this substrate (and for **Biph33** also). Nevertheless, the overall patterns of the UV–vis/CD spectra were very well reproduced and confidently confirmed the preference for the *P* (or *aR*) rotamer.

**Solvent Effects.** Because of the delicate balance among the conformers (rotamers), it seems important to check the solvent effects on the spectra experimentally (Figures S11 and S12 in Supporting Information). The effect of the solvent change (from methylcyclohexane to acetonitrile) on the observed CD spectra turned out to be not very large, and the overall pattern of the Cotton effects were not distorted for all of the three substrates. This was also checked theoretically by using a dielectric continuum solvation model, and the relative energies obtained by using the DFT-D and SCS-MP2 methods are given in Table 1. The effect of the conductor-like screening model (COSMO)<sup>24</sup> treatment on the (relative) energies was not significant and the *aR/aS* (or *P/M*) preference is only slightly altered. Nevertheless, the CD spectra predicted for all **Biph22–44** conformers by using the COSMO model (rather than the gas-phase calculations) are improved slightly and certainly better to reproduce the experi-

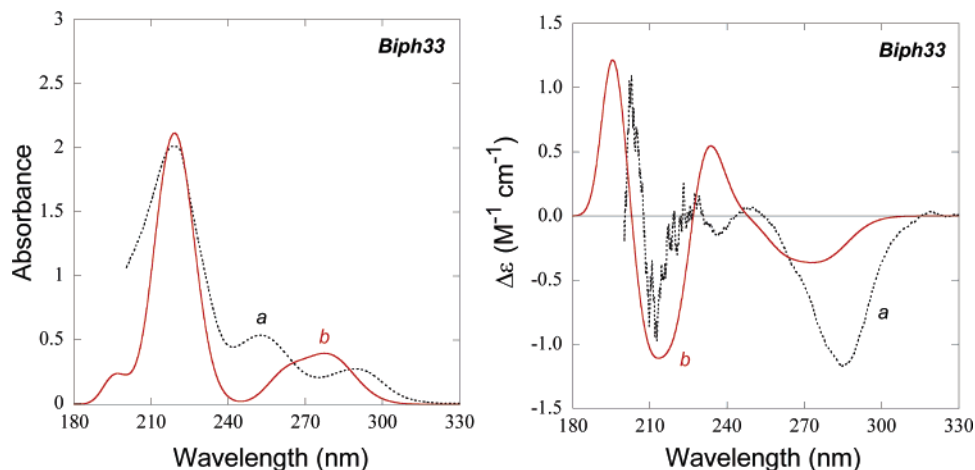


**Figure 4.** Comparison of calculated and experimental UV-vis/CD spectra of **Biph33**. Left: (a) Experimental UV-vis spectrum (0.05 mM in methylcyclohexane at 25 °C). (b) Calculated UV-vis spectrum obtained by weighted-averaging the six low-energy conformers with a scaled intensity ( $1/2$ ). Right: (a) Experimental CD spectrum. (b) Calculated CD spectra of **Biph33** obtained by weighted-averaging the six low-energy conformers with a scaled intensity ( $1/20$ ).

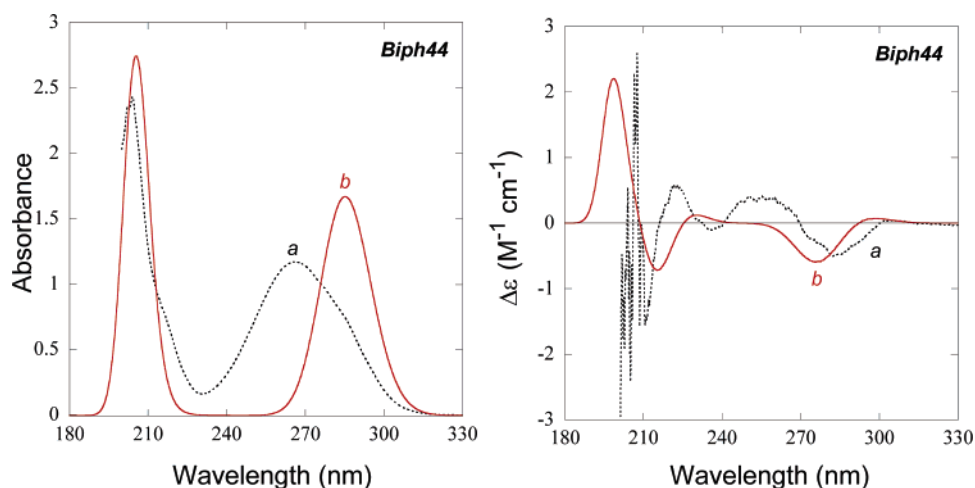


**Figure 5.** Comparison of calculated and experimental UV-vis/CD spectra of **Biph44**. Left: (a) Experimental UV-vis spectrum (0.05 mM in methylcyclohexane at 25 °C). (b) Calculated UV-vis spectrum obtained by weighted-averaging the six conformers with a scaled intensity ( $1/2$ ). Right: (a) Experimental CD spectrum. (b) Calculated CD spectra of **Biph44** obtained by weighted-averaging the six conformers with a scaled intensity ( $1/5$ ).

mental spectra in acetonitrile (Figure S11 in Supporting Information).

#### Effect of the Twist Angle on the Theoretical CD Spectra.

The effect of the ground-state geometries on the predicted CD spectra is investigated in two typical cases, that is, the *aR*-Tg-conformers of **Biph22** and **Biph44**. The structures were constructed by varying the interplanar dihedral angle by  $\pm 5$  and  $\pm 10^\circ$  from the optimized geometries. The rest of the structural parameters were kept fixed at the optimized values. Figure 6 represents the UV-vis and CD spectra predicted for the structures thus obtained with increased (red) and decreased (blue) interplanar angles. Most of the transitions in the calculated UV-vis spectra are blue-shifted to some extent for the structures with increased twisting angles, and the shift is found to be larger for the first (longer wavelength) transitions. The oscillator strengths are decreased for all the transitions in **Biph22** by increasing the twist angle but are not significantly changed in the **Biph44** case. In the CD spectra, the Cotton effects of the first and second transitions are gradually shifted to more negative values as the angle between the aromatic planes is increased. The effects of the twist angle on the high-energy CD bands are not uniform, although the shift is gradational with the degree of the twist angle.

These calculations reveal the sensitiveness of the computed CD spectra to the ground-state geometries. Thus, the accurate ground-state geometries as well as the accurate prediction of their relative energies are absolutely necessary for correctly reproducing the observed CD spectra of biphenyl derivatives.

**Calculation of Specific Rotation.** TD-DFT computation of optical rotations has become a routine tool in chiroptical studies and has frequently been employed for the prediction of absolute configuration.<sup>8,35</sup> We performed the calculation of the optical rotations of the chiral phenol ethers (**Biph22–44**) with the BH-LYP functional using the aug-cc-pVDZ basis sets (Table 1, last column). The calculated values for individual conformers are Boltzmann distribution averaged by using the most reliable single-point SCS-MP2/TZVPP energies<sup>20</sup> and are compared with the experimental values (Table 3). The calculated optical rotations for each conformer as well as the averaged ones are much larger (in absolute value) than the experimental values, although the signs of the specific rotations were correctly predicted for all three substrates (**Biph22–44**). This discrepancy is probably due to the incomplete cancellation between the conformers or ignorance of the dynamic behavior of the molecule in this static approach. In comparison to the optical rotation calculation, the CD calculation with comparable

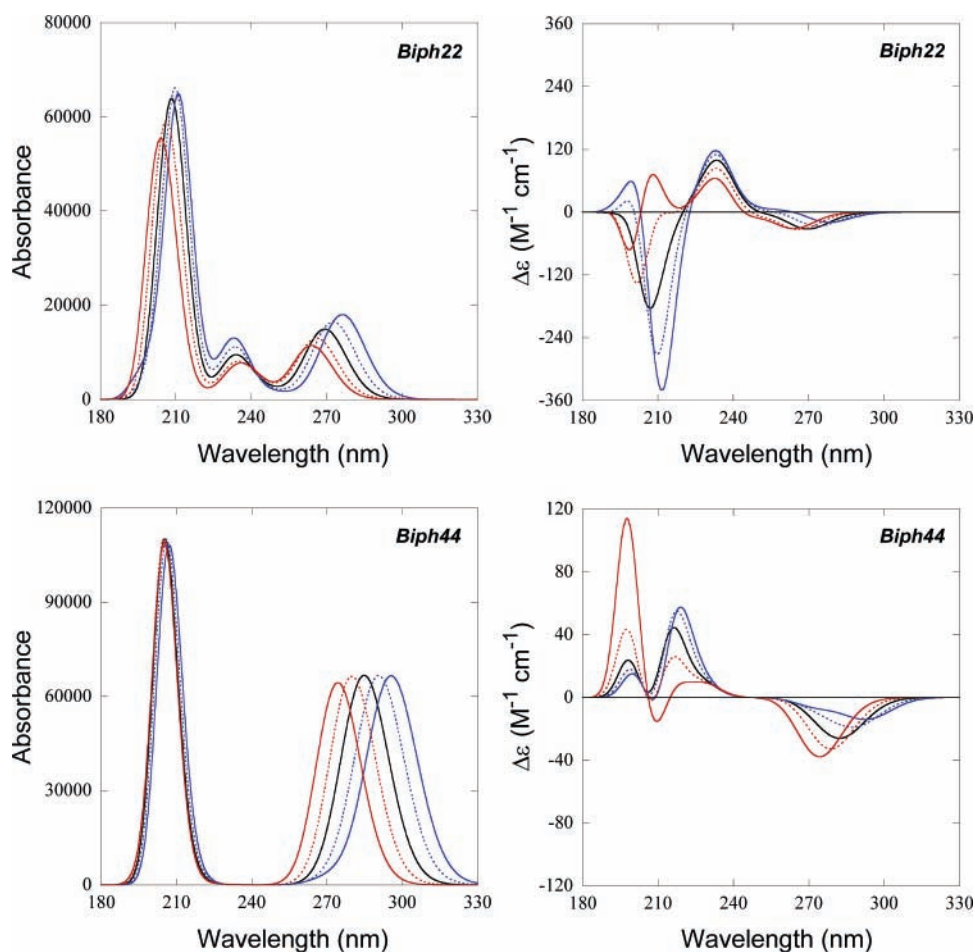


**Figure 6.** Computed UV-vis/CD spectra of **Biph22** (top) and **Biph44** (bottom) with increased and decreased dihedral angles between two aromatic planes. Black: optimized geometries. Red: structures with increased dihedral angles of  $+5^\circ$  (dotted line) and  $+10^\circ$  (solid line). Blue: structures with decreased dihedral angles of  $-5^\circ$  (dotted line) and  $-10^\circ$  (solid line).

**TABLE 3: Oxidation Potentials and Optical Rotations of Biphenol Ethers**

conformation	conformation	neutral						radical cation							
		$E_{\text{ox}}(\text{I})/\text{V vs SCE}^a$	$E_{\text{ox}}(\text{II})/\text{V vs SCE}^a$	optical rotation/ $^\circ$ <sup>c</sup>	DFT-D energy/Hartree	$\Delta E/\text{kcal mol}^{-1}$	% population	<i>R/S</i> (P/M) ratio	twist angle/ $^\circ$	DFT-D energy/Hartree	$\Delta E/\text{kcal mol}^{-1}$	% population	<i>R/S</i> (P/M) ratio	twist angle/ $^\circ$	$\Delta \text{angle}/^\circ$ <sup>d</sup>
<b>Biph22</b>	<i>aR</i>	1.28	1.35	-1000	-928.1922	$\equiv 0$	62.5	1.66	67.5	-927.9474	0.09	47.9	0.92	50.0	-17.5
	<i>aS</i>			(-33.8)	-928.1914	0.51	37.5		-90.8	-927.9475	$\equiv 0$	52.1		-45.2	-45.5
<b>Biph33</b>	<i>aR-anti</i>	1.42	1.51	-231	-928.1942	0.05	24.3	0.99	141.1	-927.9431	2.03	5.9	1.05	148.2	-7.0
	<i>aR-syn</i>			(-18.1)	-928.1942	0.00	25.5	(0.96)	-38.5	-927.9463	$\equiv 0$	45.2	(0.95)	-31.0	-7.5
	<i>aS-anti</i>				-928.1942	$\equiv 0$	25.6		-141.5	-927.9431	2.00	6.1		-148.2	-6.7
<b>Biph44</b>	<i>aS-syn</i>				-928.1942	0.04	24.6		38.8	-927.9462	0.05	42.8		31.3	-7.5
	<i>aR</i>	1.39	(1.39) <sup>b</sup>	-752	-928.1940	0.05	48.7	0.95	37.2	-927.9638	0.00	50.0	1.00	23.2	-14.0
	<i>aS</i>			(-31.3)	-928.1941	$\equiv 0$	51.3		-36.8	-927.9638	$\equiv 0$	50.0		-23.2	-13.5

<sup>a</sup> From OSWV data in dichloromethane. <sup>b</sup> Only a single two-electron oxidation peak was observed under the conditions employed. <sup>c</sup> The calculated optical rotations at the BH-LYP/aug-cc-pVDZ level were weighted with the relative population on the basis of the SCS-MP2 energies (in the gas phase). The experimental values in chloroform at 25 °C (*c* 0.10) are in parentheses. <sup>d</sup> Difference in equilibrium angle between the interplanar twists in the neutral and radical cation forms.

computation time (and level) turned out to be quite useful, since the latter gives detailed patterns (instead of just one number) that can be compared with experiment.

**Redox Properties of Biphenol Ethers.** Cyclic voltammograms were obtained for dichloromethane solutions of **Biph22**–**44** with tetrabutylammonium hexafluorophosphate as electrolyte (Figure 7). All the biphenol ethers gave irreversible redox behavior at a scan rate of 100 mV s<sup>-1</sup> under the conditions employed. Thus, the square wave voltammograms were also measured and the oxidation potentials obtained were used in the following discussion. The *para*-substituted **Biph44** showed a single oxidation peak at 1.39 V (simultaneous two-electron oxidation), which is comparable to the value reported for 4,4'-

dimethoxybiphenyl ( $E_{\text{ox}} = 1.30$  V).<sup>36</sup> The cyclic voltammograms for **Biph22** and **Biph33** showed an additional oxidation peak as a shoulder to give two sequential oxidations at  $E_{\text{ox}} = 1.28/1.35$  and 1.42/1.51 V, respectively. The relatively lower oxidation potential of **Biph22**, as compared with those reported for 2,2'- and 3,3'-dimethoxybiphenyls (1.51 and 1.60 V), may be attributed to the highly constrained ground-state geometry of **Biph22**.

**Structural Changes by Oxidation.** To gain further insight into the structural changes upon oxidation as well as the donor–acceptor interactions (vide infra), we performed geometry optimizations of the oxidized species (radical cation) for the most stable conformations (*Tg*-) of **Biph22**–**44**. The *aR*- and

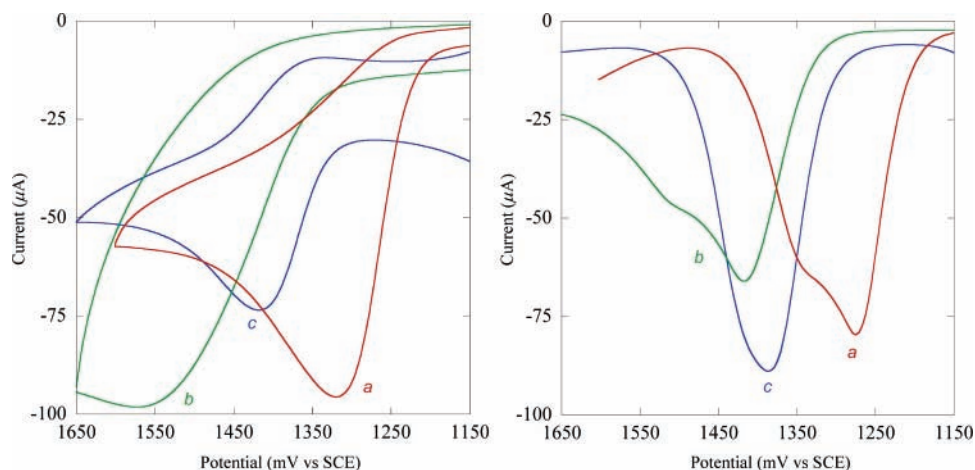


**Figure 7.** Positive scan cyclic voltammograms (left) and Osteryoung square wave voltammogram (right) of (a) **Biph22**, (b) **Biph33**, and (c) **Biph44** in dichloromethane obtained at a scan rate of  $100 \text{ mV s}^{-1}$ .

*aS*-rotamers were calculated separately, and the anti- and syn-isomers were also considered for **Biph33**. The computations for the open-shell species were performed at the unrestricted DFT-D/TZV2P level as mentioned above (Table 3). In the neutral form, the *aS*-isomer is slightly favored for **Biph44**, but the *aS/aR* ratio was found to be unity for the radical cation. The twist angle between the two aromatic planes becomes slightly smaller to give better electronic resonances between the aromatic units in the oxidized forms. Although the *P/M* value was not significantly changed for **Biph33** by oxidation, the greater preference of the syn-isomer over the anti-isomer in the radical cations is evident (Table 3). This is probably due to the larger resonances between the aromatic rings in the syn forms. The difference in twist angle was found to be small ( $7\sim 8^\circ$ ) between the neutral and radical cationic species. The largest geometrical changes upon oxidation are expected to occur for **Biph22**, and indeed the calculated change of the twist angle was found to be quite large ( $18^\circ$  and  $46^\circ$  for *aR*- and *aS*-isomers, respectively). Accordingly, the preference for the less strained *aS*-isomer in the radical cation form is considerable. Thus, the relatively low oxidation potential of **Biph22** can be ascribed to the higher strain in the neutral form.

**Donor–Acceptor Complexation of the Chiral Ethers with Various Electron Acceptors.** **Biph22–44** can form donor–acceptor (or charge transfer) complexes with electron acceptors. Accordingly, addition of various acceptors to solutions of **Biph22–44** led to colorful solutions as shown in Figure 8 (bottom) (also see Figure S16). Subtraction of the reference spectra of free donor and acceptor from that of the mixed solution reveals the CT bands in the visible region. The pattern of the CT transitions critically depends on the choice of donor and acceptor. The HOMO–LUMO transition (the first CT transition) always appears at longer wavelengths not for **Biph22** or **Biph33** but for **Biph44**, which is, however, not the most easily oxidizable substrate (**Biph22** has a lower oxidation potential). The shape of the CT bands obtained with **Biph22** and **Biph33** was quite similar to each other for all the acceptors examined (see Figure S13 in Supporting Information). These observations indicate that large geometrical changes in donor structure, which are significantly different among **Biph22–44**, should be accompanied upon CT complexation.

We have recently demonstrated that the Cotton effects observed for the CT transitions in donor–acceptor complexes can be utilized to detect the conformational and configurational changes of the complex.<sup>12,37</sup> Despite the large differences in color (or in excitation energy), the CD spectra observed for the

CT transitions do not greatly differ in sign and pattern among the CT complexes of **Biph22–44** with tetracyanoethylene (Figure 8, left). Similar results were also obtained for the complexes with benzoquinone and with chloranil (see Figures S14 and S15 in Supporting Information). However, the observed Cotton effect was very sensitive to the shape of the CT complex formed. Thus, the CD spectra of **Biph22–44** complexes with dimethylviologen were shown to be highly dependent on the donor structure (Figure 8, right). The ground-state geometry of the CT complex of dimethylviologen and 4,4'-biphenol was recently optimized at the B3-LYP/6-311G(d) level, and the result indicates that the two aromatic planes in each component are coplanar to each other and that the donor–acceptor pair is placed in a face-to-face configuration.<sup>38</sup> A similar configuration is also expected for a complex of **Biph44** with dimethylviologen but not for complexes of **Biph22** and **Biph33** because of the twisting nature and steric requirements of the ground-state conformations of biphenol ethers **Biph22** and **Biph33**. Although detailed investigations of the CD spectra of the complex remain to be elucidated, such Cotton effects observed at the CT band of chiral CT complex contain the wealth of structural information and would be potentially useful for the structural analysis of the complex in solution.

#### 4. Summary and Conclusions

In the present study, we have comprehensively investigated the chiroptical properties of three chiral biphenyl derivatives (**Biph22–44**) both experimentally and theoretically. It was found that our static approach (on the basis of the thermally populated conformers of minimum energies) to predict CD spectra is very robust and applicable even to these conformationally flexible systems. The following findings are crucial:

(1) A pair of small peripheral chiral auxiliaries induce noticeable axial chirality in biphenyls (**Biph22–44**). The observed Cotton effects are very small in intensity because of the cancellation of the signals among the rotamers, giving  $\Delta\epsilon = 2\sim 8$  for **Biph22** and  $\Delta\epsilon \sim 1$  for **Biph33** and **Biph44**. In **Biph22**, chiral groups are located much closer to the axes of the biphenyl than in **Biph33** or **Biph44**, which induces stronger Cotton effects in CD.

(2) The calculation at the dispersion-corrected DFT-D-B-LYP/TZV2P level is suitable for the geometry optimizations of **Biph22–44**. The interplanar angles of the optimized geometries are in good agreement with the experimental values reported for analogous biphenyl derivatives. The following

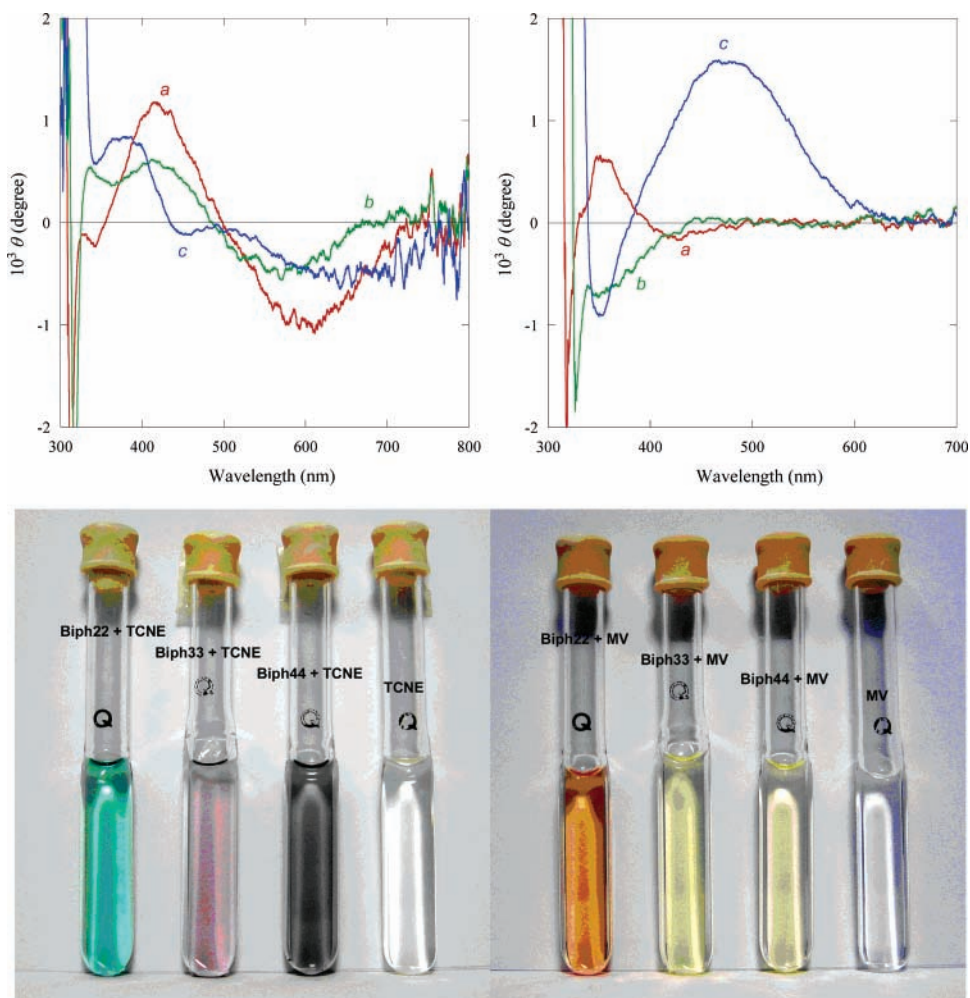


**Figure 8.** CD spectra of CT complexes. Top, left: Tetracyanoethylene (TCNE, 0.1 M) with (a) **Biph22** (50 mM), (b) **Biph33** (10 mM), and (c) **Biph44** (10 mM) in dichloromethane at 25 °C. Top, right: Dimethylviologen (MV, 50 mM) with (a) **Biph22** (0.4 M), (b) **Biph33** (0.2 M), and (c) **Biph44** (0.2 M) in acetonitrile at 25 °C. Bottom: Color changes for the CT complex formation between **Biph22–44** with TCNE or MV.

single-point SCS-MP2/TZVPP energy calculations revealed that the geometries obtained by DFT-D method are accurate enough to further simulate the chiroptical properties. The empirical dispersion correction in DFT was found to be important in particular for **Biph22**, where the most significant intramolecular steric interactions are anticipated. The steric hindrance of the alkoxy groups in **Biph22** also affects the electrochemical behavior. Thus, the oxidation of **Biph22** is irreversible and occurs at a potential ( $E_{\text{ox}}(\text{I}) = 1.28 \text{ V}$ ) smaller than that for **Biph33** or **biph44** ( $E_{\text{ox}}(\text{I}) > \sim 1.4 \text{ V}$ ).

(3) From the results of the TD-DFT simulation of CD spectrum on the basis of the SCS-MP2 energies of all possible conformers of **Biph22**, we can conclude that the effect of minor conformers on the averaged UV-vis/CD spectrum is trivial. Hence, only the  $Tg+$ ,  $Tg-$ , and  $G+t$  conformers being taken into account, the UV-vis/CD spectra and optical rotations of respective conformers are calculated at the TD-DFT-BH-LYP/TZV2P and BH-LYP/aug-cc-pVDZ levels to give satisfactory results. Most interestingly, the pairs of rotamers yield almost mirror-imaged CD profiles (except for the  $Tg-$  conformer of **Biph22**). From the comparison of the SCS-MP2 energies, it turned out that most of the rotamers (with the same conformation of the alkyl group) have very similar stability, but a slight preference for one of the rotamers is exaggerated in the overall averaged CD spectrum. Most crucially, the calculated CD spectra are in excellent agreement with the experimental ones

in pattern and relative intensity. However, the observed rotatory strengths are always smaller ( $1/5 \sim 1/20$ ) than the theoretical values. This is probably due to the ignorance of the dynamic behavior, which leads to the incomplete cancellation, in our static approach, where the vibrational wavefunctions are not considered.

(4) Both the experimental and theoretical CD spectra indicate that (*R,R*)-**Biph33** and (*R,R*)-**Biph44** slightly favor the (*M*)-isomers in solution, while (*R,R*)-**Biph22**, possessing the same chiral auxiliaries, prefers the opposite (*P*)-isomer, probably owing to the more severe steric hindrance.

(5) Solvent effects are insignificant on both experimental and theoretical CD spectra. Consequently, the use of the COSMO model in the calculations of relative energy and population gives better fits to the experimental CD spectra in acetonitrile.

(6) **Biph22–44** form CT complexes with a variety of electron acceptors in solution. The geometry of the complex and thus the observed CD spectral shape of the CT band are highly dependent on the combination of the donor and the acceptor. The CD spectral changes associated with the CT complex formation are potentially useful for obtaining the conformational information of the complexes as well as the parent molecules in the condensed phase.

Despite the fact that biphenyl molecules are in dynamic equilibrium with varying interplanar angles in solution, our static approach simply on the basis of the pairs of rotamers at the

local minima can nicely reproduce the experimental CD spectra. In the present case, the slight preference for one rotamer is easily deduced by a comparison of the experimental and theoretical CD spectra. We conclude therefore that the combined use of the geometry optimization by DFT-D, single-point energy calculation by SCS-MP2, and CD simulation by TD-DFT with basis sets of (properly polarized) triple- $\zeta$  quality is a robust and potent protocol for the conformational analysis of flexible chiral molecules in solution executable at quite reasonable computational cost and therefore has bright perspective for further applications.

**Acknowledgment.** T.M. thanks the Alexander von Humboldt-Stiftung for the fellowship. We thank Drs. Christian Mück-Lichtenfeld, Christian Diedrich, and Manuel Piacenza for technical assistance and fruitful discussion. Financial support of this work by a Grant-in-Aid for Scientific Research from the Ministry of Education, Culture, Sports, Science, and Technology of Japan to T.M. is gratefully acknowledged.

**Supporting Information Available:** General experimental details,  $^1\text{H}$  and  $^{13}\text{C}$  NMR spectra of all compounds in this study, detailed investigation of the CD spectra of **Biph22**, bar representation of the calculated excitation energies and rotational strength of the transition for *aR-Tg*- conformers of **Biph22-44**, comparison of experimental and calculated CD spectra in acetonitrile, UV-vis/CD spectra, anisotropy factors, and color changes of CT complex formation, and Cartesian coordinates of the optimized geometries of a variety of conformations of **Biph22-44** and complete ref 14. This material is available free of charge via the Internet at <http://pubs.acs.org>.

## References and Notes

- Kenner, J.; Stubbings, W. V. *J. Am. Chem. Soc.* **1921**, *119*, 593–602.
- For reviews, see: (a) Bringmann, G.; Mortimer, A. J. P.; Keller, P. A.; Greser, M. J.; Garner, J.; Breuning, M. *Angew. Chem., Int. Ed.* **2005**, *44*, 5384–5427. (b) Baudoin, O. *Eur. J. Org. Chem.* **2005**, 4223–4229. (c) Bringmann, G.; Menche, D. *Acc. Chem. Res.* **2001**, *34*, 615–624.
- (a) Honda, K.; Furukawa, Y. *J. Mol. Struct.* **2005**, 735–736, 11–19. (b) Zhuravlev, K. K.; McCluskey, M. D. *J. Chem. Phys.* **2004**, *120*, 1841–1845. (c) Gullion, T.; Conradi, M. S. *Phys. Rev. B* **1984**, *30*, 1133–7. (d) Bouzakraoui, S.; Bouzzine, S. M.; Bouachrine, M.; Hamidi, M. *Phys. Chem. News* **2004**, *19*, 104–109. (e) Murthy, P. S.; Michl, J. *Collect. Czech. Chem. Commun.* **1988**, *53*, 2366–76.
- (a) Berova, N.; Nakanishi, K.; Woody, R. W. *Circular Dichroism, Principles and Applications*, 2nd ed.; John Wiley & Sons: New York, 2000. (b) Lightner, D. A.; Gurst, J. E. *Organic Conformational Analysis and Stereochemistry from Circular Dichroism Spectroscopy*; John Wiley & Sons: New York, 2000.
- For example, see: (a) Smith, H. E. *Chem. Rev.* **1998**, *98*, 1709–1740. (b) Moffitt, W.; Woodward, R. B.; Moscovitz, A.; Klyne, W.; Djerassi, C. *J. Am. Chem. Soc.* **1961**, *83*, 4013–4018. (c) Harada, N.; Nakanishi, K. *J. Am. Chem. Soc.* **1969**, *91*, 3989–3991. (d) Smith, H. E.; Neergaard, J. R.; Burrows, E. P.; Chen, F.-M. *J. Am. Chem. Soc.* **1974**, *96*, 2908–2916.
- Superchi, S.; Casarini, D.; Laurita, A.; Bavoso, A.; Rosini, C. *Angew. Chem., Int. Ed.* **2001**, *40*, 451–454.
- For an example of failure of such empirical methods to predict the absolute configuration of simple but electronically perturbed systems (i.e., donor–acceptor cyclophanes), see: Furo, T.; Mori, T.; Wada, T.; Inoue, Y. *J. Am. Chem. Soc.* **2005**, *127*, 8242–8243, 16338.
- For recent examples, see: (a) Mort, B. C.; Autschbach, J. *J. Phys. Chem. A* **2006**, *110*, 11381–11383. (b) Kundrat, M. D.; Autschbach, J. *J. Phys. Chem. A* **2006**, *110*, 4115–4123. (c) Autschbach, J.; Jensen, L.; Schatz, G. C.; Tse, Y. C. E.; Krykunov, M. *J. Phys. Chem. A* **2006**, *110*, 2461–2473. (d) Durandin, A.; Jia, L.; Crean, C.; Kolbanovskiy, A.; Ding, S.; Shafirovich, V.; Brojde, S.; Geacintov, N. E. *Chem. Res. Toxicol.* **2006**, *19*, 908–913. (e) Giorgio, E.; Roje, M.; Tanaka, K.; Hamersak, Z.; Sunjic, V.; Nakanishi, K.; Rosini, C.; Berova, N. *J. Org. Chem.* **2005**, *70*, 6557–6563. (f) Crawford, T. D.; Owens, L. S.; Tam, M. C.; Schreiner, P. R.; Koch, H. *J. Am. Chem. Soc.* **2005**, *127*, 1368–1369.
- (9) For recent examples, see: (a) Carosati, E.; Cruciani, G.; Chiarini, A.; Budriesi, R.; Ioan, P.; Spisani, R.; Spinelli, D.; Cosimelli, B.; Fusi, F.; Frosini, M.; Maticci, R.; Gasparini, F.; Ciogli, A.; Stephens, P. J.; Devlin, F. J. *J. Med. Chem.* **2006**, *49*, 5206–5216. (b) Kuppens, T.; Herrebout, W.; van der Veken, B.; Bultinck, P. *J. Phys. Chem. A* **2006**, *110*, 10191–10200. (c) Munoz, M. A.; Munoz, O.; Joseph-Nathan, P. *J. Nat. Prod.* **2006**, *69*, 1335–1340. (d) Brotin, T.; Cavagnat, D.; Dutasta, J.-P.; Buffeteau, T. *J. Am. Chem. Soc.* **2006**, *128*, 5533–5540. (e) Longhi, G.; Abbate, S.; Gangemi, R.; Giorgio, E.; Rosini, C. *J. Phys. Chem. A* **2006**, *110*, 4958–4968. (f) Fristrup, P.; Lassen, P. R.; Johannessen, C.; Tanner, D.; Norrby, P.-O.; Jalkanen, K. J.; Hemmingsen, L. *J. Phys. Chem. A* **2006**, *110*, 9123–9129. (g) Tarczay, G.; Magyarfalvi, G.; Vass, E. *Angew. Chem., Int. Ed.* **2006**, *45*, 1775–1777. (h) Brotin, T.; Cavagnat, D.; Dutasta, J.-P.; Buffeteau, T. *J. Am. Chem. Soc.* **2006**, *128*, 5533–5540. (i) Monde, K.; Taniguchi, T.; Miura, N.; Vairappan, C. S.; Suzuki, M. *Chirality* **2006**, *18*, 335–339. (j) Naubron, J.-V.; Giordano, L.; Fotiadu, F.; Buergi, T.; Vanthuyne, N.; Roussel, C.; Buono, G. *J. Org. Chem.* **2006**, *71*, 5586–5593. (k) Shin, S.; Nakata, M.; Hamada, Y. *J. Phys. Chem. A* **2006**, *110*, 2122–2129. (l) Vargas, A.; Bonalumi, N.; Ferri, D.; Baiker, A. *J. Phys. Chem. A* **2006**, *110*, 1118–1127. (m) Devlin, F. J.; Stephens, P. J.; Besse, P. *J. Org. Chem.* **2005**, *70*, 2980–2993. (n) Devlin, F. J.; Stephens, P. J.; Bortolini, O. *Tetrahedron: Asymmetry* **2005**, *16*, 2653–2663. (o) Devlin, F. J.; Stephens, P. J.; Besse, P. *Tetrahedron: Asymmetry* **2005**, *16*, 1557–1566.
- (10) For recent examples, see: (a) McCann, D. M.; Stephens, P. J. *J. Org. Chem.* **2006**, *71*, 6074–6098. (b) Stephens, P. J.; McCann, D. M.; Devlin, F. J.; Smith, A. B., III. *J. Nat. Prod.* **2006**, *69*, 1055–1064. (c) Gawronski, J. K.; Kwit, M.; Boyd, D. R.; Sharma, N. D.; Malone, J. F.; Drake, A. F. *J. Am. Chem. Soc.* **2005**, *127*, 4308–4319. (d) Schühly, W.; Crockett Sara, L.; Fabian Walter, M. F. *Chirality* **2005**, *17*, 250–256. (e) Forzato, C.; Furlan, G.; Nitti, P.; Pitacco, G.; Marchesan, D.; Coriani, S.; Valentin, E. *Tetrahedron: Asymmetry* **2005**, *16*, 3011–3023. (f) Zuber, G.; Goldsmith, M.-R.; Hopkins, T. D.; Beratan, D. N.; Wipf, P. *Org. Lett.* **2005**, *7*, 5269–5272. (g) Stephens, P. J.; McCann, D. M.; Cheeseman, J. R.; Frisch, M. J. *Chirality* **2005**, *17*, S52–S64.
- (11) (a) Diedrich, C.; Grimme, S. *J. Phys. Chem. A* **2003**, *107*, 2524–2539. (b) Autschbach, J.; Ziegler, T.; van Gisbergen, S. J. A.; Baerends, E. *J. J. Chem. Phys.* **2002**, *116*, 6930–6940.
- (12) (a) Mori, T.; Inoue, Y.; Grimme, S. *J. Org. Chem.* **2006**, *71*, 9797–9806. See also: (b) Mori, T.; Ko, Y. H.; Kim, K.; Inoue, Y. *J. Org. Chem.* **2006**, *71*, 3232–3247. (c) Mori, T.; Inoue, Y. *Angew. Chem., Int. Ed.* **2005**, *44*, 2582–2585.
- (13) (a) Mitsunobu, O. *Synthesis* **1981**, 1–28. (b) Huges, D. L. *Org. Prep. Proced. Int.* **1996**, *28*, 127–164. (c) Dodge, J. A.; Jones, S. A. *Rec. Res. Dev. Org. Chem.* **1997**, *1*, 273–283.
- (14) Ahlrichs, R. et al. *TURBOMOLE*, version 5.8; Universität Karlsruhe: Karlsruhe, 2005. See also: [http://www.cosmologic.de/QuantumChemistry/main\\_turbomole.html](http://www.cosmologic.de/QuantumChemistry/main_turbomole.html).
- (15) (a) Eichkorn, K.; Treutler, O.; Öhm, H.; Häser, M.; Ahlrichs, R. *Chem. Phys. Lett.* **1995**, *240*, 283–289. (b) Weigend, F.; Häser, M. *Theor. Chem. Acc.* **1997**, *97*, 331–340. (c) Grimme, S.; Waletzke, M. *Phys. Chem. Chem. Phys.* **2000**, *2*, 2075–2081. (d) Vahtras, O.; Almlöf, J.; Feyereisen, M. W. *Chem. Phys. Lett.* **1993**, *213*, 514–518.
- (16) Hättig, C.; Weigend, F. *J. Chem. Phys.* **2000**, *113*, 5154–5161.
- (17) Bauernschmidt, R.; Ahlrichs, R. *Chem. Phys. Lett.* **1996**, *256*, 454–464.
- (18) Grimme, S. *J. Comput. Chem.* **2004**, *25*, 1463–1473.
- (19) (a) Grimme, S. *J. Phys. Chem. A* **2005**, *109*, 3067–3077. (b) Goumans, T. P. M.; Ehlers, A. W.; Lammertsma, K.; Würthwein, E.-U.; Grimme, S. *Chem. Eur. J.* **2004**, *10*, 6468–6475. (c) Grimme, S. *J. Chem. Phys.* **2003**, *118*, 9095–9102.
- (20) (a) Grimme, S. *J. Comput. Chem.* **2003**, *24*, 1529–1537. (b) Piacenza, M.; Grimme, S. *J. Comput. Chem.* **2004**, *25*, 83–99. (c) Gerenkamp, M.; Grimme, S. *Chem. Phys. Lett.* **2004**, *392*, 229–235.
- (21) (a) Grimme, S. *Angew. Chem., Int. Ed.* **2006**, *45*, 4460–4464 and references cited therein. (b) Grimme, S.; C. Diedrich, S.; Korth, M. *Angew. Chem., Int. Ed.* **2006**, *45*, 625–629.
- (22) Notations from Gaussian package corresponds to BH&HLYP. See also: (a) Maity, D. K.; Duncan, W. T.; Truong, T. N. *J. Phys. Chem. A* **1999**, *103*, 2152–2159. (b) Duncan, W. T.; Truong, T. N. *J. Chem. Phys.* **1995**, *103*, 9642–9652. (c) Liao, M.-S.; Lu, Y.; Scheiner, S. *J. Comput. Chem.* **2003**, *24*, 623–631.
- (23) (a) Dunning, T. H. *J. Chem. Phys.* **1993**, *98*, 7059–7071. (b) Kendall, R. A.; Dunning, T. H.; Harrison, R. J. *J. Chem. Phys.* **1992**, *96*, 6796–6806.
- (24) (a) Klamt, A.; Schüürmann, G. P. *J. Chem. Soc., Perkin Trans. 2* **1993**, 799–805. (b) Tomasi, J.; Persico, M. *Chem. Rev.* **1994**, *94*, 2027–2094. (c) Sinnecker, S.; Rajendran, A.; Klamt, A.; Diedenhofen, M.; Neese, F. *J. Phys. Chem. A* **2006**, *110*, 2235–2245. See also: (d) Pecul, M.; Marchesan, D.; Ruud, K.; Coriani, S. *J. Chem. Phys.* **2005**, *122*, 024106.

- (25) Baumer, V. N.; Doroshenko, A. O.; Verezubova, A. A.; Ptyagina, L. M.; Kirichenko, A. V.; Ponomarev, O. A. *Khim. Geterotsykl. Soedin.* **1996**, 984–991.
- (26) (a) Piacenza, M.; Grimme, S. *J. Am. Chem. Soc.* **2005**, *127*, 14841–14848. (b) Piacenza, M.; Grimme, S. *Chem. Phys. Chem.* **2005**, *6*, 1554–1558. (c) Antony, J.; Grimme, S. *Phys. Chem. Chem. Phys.* **2006**, *8*, 5287–5293.
- (27) Parac, M.; Etinski, M.; Peric, M.; Grimme, S. *J. Chem. Theory Comput.* **2005**, *1*, 1110–1118.
- (28) For a recent overview, see: Grimme, S.; Antony, J.; Schwabe, T.; Mück-Lichtenfeld, C. *Org. Biomol. Chem.* **2007**, *5*, 741–758.
- (29) For stereodescriptors of the axial chirality, see: Moss, G. P. *Pure Appl. Chem.* **1996**, *68*, 2193–2222.
- (30) (a) Furche, F.; Ahlrichs, R.; Wachsmann, C.; Weber, E.; Sobanski, A.; Vogtle, F.; Grimme, S. *J. Am. Chem. Soc.* **2000**, *122*, 1717–1724. (b) Autschbach, J.; Ziegler, T.; van Gisbergen, S. J. A.; Baerends, E. J. *J. Chem. Phys.* **2002**, *116*, 6930–6940. (c) Pecul, M.; Ruud, K.; Helgaker, T. *Chem. Phys. Lett.* **2004**, *388*, 110–119.
- (31) Mori, T.; Inoue, Y.; Grimme, S. submitted for publication.
- (32) Roberts, R. M. G. *Magn. Reson. Chem.* **1985**, *23*, 52–4.
- (33) (a) Schreiner, P. R.; Fokin, A. A.; Pascal, R. A.; deMeijere, A. *Org. Lett.* **2006**, *8*, 3635–3638. (b) Wodrich, M. D.; Corminboeuf, C.; Schleyer, P. v. R. *Org. Lett.* **2006**, *8*, 3631–3634. (c) Check, C. E.; Gilbert, T. M. *J. Org. Chem.* **2005**, *70*, 9828–9834. (d) On the contrary, see: Moran, D.; Simmonett, A. C.; Leach, F. E., III; Allen, W. D.; Schleyer, P. v. R.; Schaefer, H. F., III. *J. Am. Chem. Soc.* **2006**, *128*, 9342–9343.
- (34) Suzuki, H. *J. Phys. Chem.* **1959**, *32*, 1340–1350.
- (35) (a) Grimme, S.; Furche, F.; Ahlrichs, R. *Chem. Phys. Lett.* **2002**, *361*, 321–328. (b) Grimme, S. *Chem. Phys. Lett.* **2001**, *339*, 380–388. (c) Ruud, K.; Helgaker, T. *Chem. Phys. Lett.* **2002**, *352*, 533–539. (d) Autschbach, J.; Patchkovskii, S.; Ziegler, T.; van Gisbergen, S. J. A.; Baerends, E. J. *J. Chem. Phys.* **2002**, *117*, 581–592. (e) Stephens, P. J.; Devlin, F. J.; Cheeseaman, J. R.; Frisch, M. J. *J. Phys. Chem. A* **2001**, *105*, 5356–5379.
- (36) Fisher, G. J.; LeBlanc, J. C.; Johns, H. E. *Photochem. Photobiol.* **1967**, *6*, 757–767.
- (37) (a) Briegleb, G.; Kuballe, H. G. *Angew. Chem., Int. Ed. Engl.* **1964**, *3*, 307–308. (b) Briegleb, G.; Kuballe, H. G.; Henschel, K. *J. Phys. Chem. (Frankfurt)* **1965**, *46*, 229–249. (c) Briegleb, G.; Kuballe, H. G.; Henschel, K.; Euing, W. *Ber. Bunsen-Ges. Phys. Chem.* **1972**, *76*, 101–105. (d) Wynberg, H.; Lammertsma, K. *J. Am. Chem. Soc.* **1973**, *95*, 7913–7914. (e) Geissler, U.; Schulz, R. C. *Makromol. Chem. Rapid Commun.* **1981**, *2*, 591–594.
- (38) (a) Moran, A. M.; Aravindan, P.; Spears, K. G. *J. Phys. Chem. A* **2005**, *109*, 1795–1801. See also: (b) Ponnau, A.; Sung, J.; Spears, K. G. *J. Phys. Chem. A* **2006**, *110*, 12372–12384.